COBEM 2023 27TH INTERNATIONAL CONGRESS OF MECHANICAL ENGENEERING

ABCM Brazilian Society of Mechanical Sciences and Engineering
27th ABCM International Congress of Mechanical Engineering
December 04-08, 2023, Florianópolis-SC, Brazil

COB2023-0690
NUMERICAL INVESTIGATION OF DROPLET DEFORMATION AND BREAKUP IN T-JUNCTION MICROFLUIDICS

Juan Linhares Barbosa
Laboratory of Energy and Environment, Department of Mechanical Engineering, University of Brasília, Brasília DF 70910-900, Brazil
juanlinhares123@gmail.com
Paulo Henrique Neves Pimenta
Department of Academic Areas IV, Federal Institute of Goiás, Goiânia GO 74055-110, Brazil
paulo.pimenta@ifg.edu.br
Taygoara Felamingo de Oliveira
Laboratory of Energy and Environment, Department of Mechanical Engineering, University of Brasília, Brasília DF 70910-900, Brazil
taygoara@unb.br

Abstract. *Understanding the flow, deformation, and breakup of droplets in T-junctions is essential for generating monodisperse emulsions in microfluidic devices. In this study, we developed a model based on the Navier-Stokes equation and the Level Set method to analyze the behavior of droplets in a T-junction. By comparing our results with literature references, we validated our model's accuracy for both the inlet and outlet regions of the T-junction. We found that the deformation of droplets in the main channel depends on their size and the capillary number. Small droplets result in minimal deformations, while larger droplets lead to significant deviations from the spherical shape. Decreasing the capillary number reduces deformation due to increased interfacial tension. Furthermore, we observed that elongated droplets experience higher mean velocities along the main channel for larger capillary numbers. In terms of breakup, elongated droplets tend to fragment into smaller ones at higher capillary numbers. Our findings highlight the crucial role of the capillary number in governing droplet behavior and breakup in the T-junction. Overall, this study provides valuable insights into controlling and understanding emulsions in microfluidic devices, benefiting various industrial processes.*

Keywords: *biphasic flow, droplet confinament, droplet breakup, level set method, emulsion generation*

1. INTRODUCTION

There are extensive studies dedicated to investigating the dynamics of droplet deformation and breakup in unconfined extensional and simple shear flows. The literature dates back to Taylor (1932), who initially calculated the viscosity of small spherical drops with high surface tension. Subsequently, Taylor (1934) conduced experiments for the distortion of a drop in regimes of flow with both low and high speeds. In the range of low speeds, there was a good agreement with the theory of small deformations and the drops keep it shape almost spherical. For higher speeds, the deformation of the droplets varies greatly with the ratio of viscosity λ and the capillary number Ca. It has been shown that for small values of λ, the droplet becomes elongated until a critical speed, from which the elongation ceases and it reaches a steady elongated shape. As λ increases, the droplet burst for some less speed of the flow.

Some theoretical studies involving the geometry of two-dimensional bubbles are performed by Richardson (1968) for pure strain motion and simple shear flows. After that, Richardson (1973) studied the geometry of bubbles in parabolic flow and obtained that the shape of bubble's surface is greatly influenced by its initial radius and the capillary number. Richardson also demonstrated that bubble placed at the center of the parabolic flow move fastly than the undisturbed flow.

Opposite to unconfined flows, the understanding of droplet dynamics in microfluidic devices, which offer confinement for the droplets, is crucial for various industrial processes involving emulsions. a divergente T-junction can play a similar role as extensional confined flows, where a droplet is pushed by equal branches and get elongated. Depending on the length of the droplet and the capillary number, Jullien *et al.* (2009) classified the breakup of droplets into two regimes and one non-breakup regime: (a) existence of thin film (tunnel) between the droplet and the T-junction wall before breakup and (b) no tunnel regime, in which droplets obstruct permanently the channel before breakup. In the non-breakup regime (c), the droplet reaches a steady state elongation and eventually escapes into one of the branches of the T-junction. The experiments of Link *et al.* (2004) allowed to propose an analytical model to understand the breaking to nonbreaking transition of droplets that relates the capillary number with the droplet's initial extension ℓ_0/w in a T-junction with channel width w. The studies of Leshansky and Pismen (2009) extended this analysis to obtain a theoretical model for the droplet breaking prediction combining a geometric construction of the droplet shape with a lubrication theory in the thin film between the droplet and the channel wall. This model was obtained for the limit of low capillary number. Afkhami *et al.* (2011) performed numerical simulations to compare the previous theoretical prediction for a range of capillary number,

showing that the theory also has a good agreement with larger capillary number.

The breakup mechanism can also be influenced by capillary instability, as investigated by the study conducted by Link *et al.* (2004). When droplets become excessively elongated, they undergo the Rayleigh-Plateau phenomenon, where a cylindrical liquid thread can decrease its overall surface area by breaking it in small drops when its length surpasses its circumference. However, it is important to note that this mechanism is primarily three-dimensional, whereas in two-dimensional theoretical models by Leshansky and Pismen and numerical simulations by Afkhami *et al.* the dominant cause of breakup is flow-driven. Therefore, the Rayleigh-Plateau instability is not actively involved in breakup analysis in the simulations presented in this work as well.

While different numerical techniques have been employed to study the behavior of droplets in microfluidics, such as VOF (Volume of Fluid) approach performed by Leshansky and Pismen, this work also address it providing another technique. By presenting a numerical methodoly using the Level-set method for evolving the interface of a droplet undergoing a pressure-driven flow within a continuous fluid along a T-Junction configuration, our study contributes to the advancement of understanding and controlling emulsions in microfluidic devices, where the manipulation and stability of emulsions play a critical role.

2. PROBLEM STATEMENT

We have considered a single droplet placed in the main channel of a T-junction surrounded by an immiscible Newtonian incompressible fluid with viscosity μ_1 and density ρ_1. The study was carried out using a two-dimensional domain in which there is an inlet region with an uniform velocity $\boldsymbol{U}$ and an outlet region with hydrodynamic fully developed flow condition for velocity (i.e. $\nabla \boldsymbol{u} \cdot \hat{\boldsymbol{n}} = 0$). Initially, the droplet is elliptic with major semiaxis a in the same direction of $x-$axis and its center is located at the symmetric axis of the main channel as showed in Fig 1. The droplet's fluid is also Newtonian incompressible with density $\rho_2 = \rho_1$ and viscosity μ_2. The droplet interface is assumed to be free of tensioactive substances, which means that it has a constant surface tension coefficient σ. Moreover, the T-junction dimensions are defined by lengths L_x and L_y and width H for both the main and outer channels.

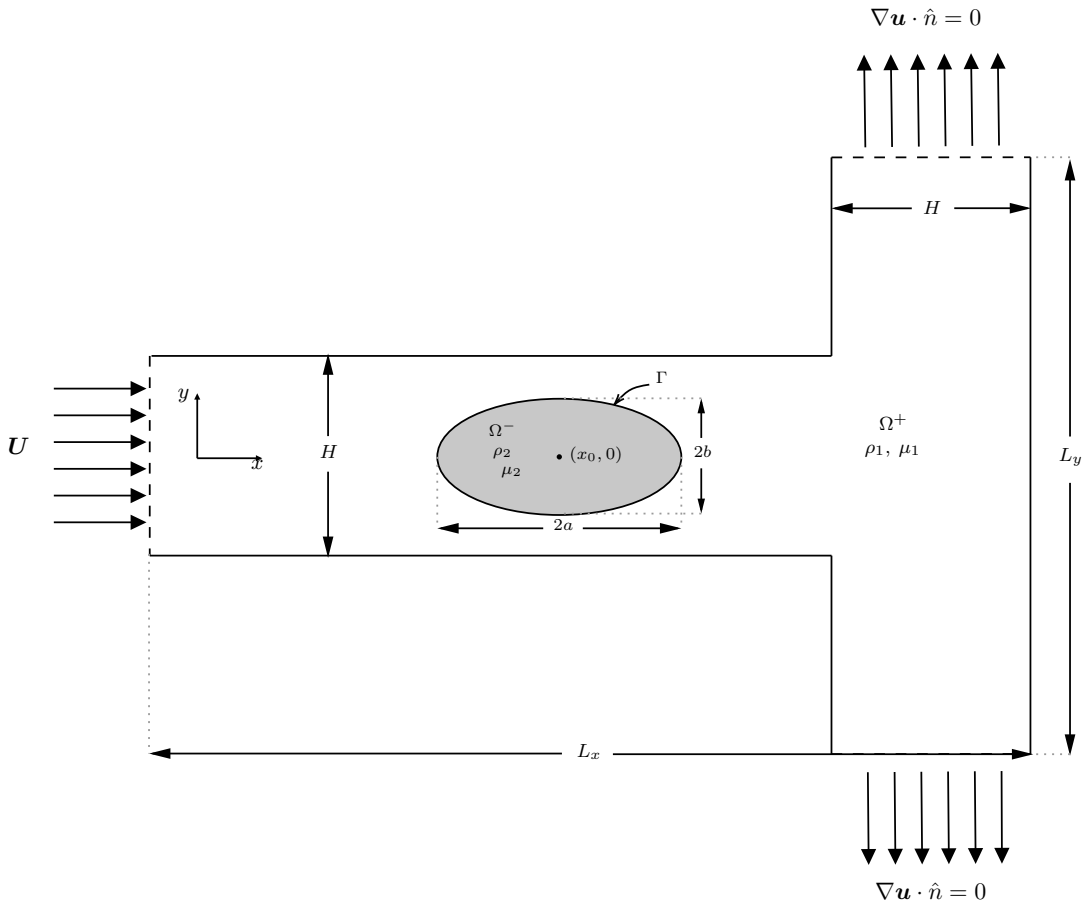

Figure 1: Schematic illustration for the droplet placed in a T-junction configuration.

2.1 Governing equations

The physics of two-phase flow involving two immiscible and viscous fluid is tipically governed by the incompressible Navier-Stokes equations, accounting the capillary force $\boldsymbol{F_\sigma}$ due to the presence of an interface separating both phases. Therefore,

$$\nabla \cdot \boldsymbol{u} = 0 \tag{1}$$

and

$$\rho \left(\frac{\partial \boldsymbol{u}}{\partial t} + \boldsymbol{u} \cdot \nabla \boldsymbol{u} \right) = -\nabla p + \mu \nabla^2 \boldsymbol{u} + \boldsymbol{F_\sigma}, \tag{2}$$

where $\boldsymbol{u}$ is the velocity field, t is time and p is the pressure field. The interfacial force is given by

$$\boldsymbol{F_\sigma} = -\sigma \kappa \delta(\phi) |\nabla \phi| \hat{\boldsymbol{n}}, \tag{3}$$

where κ is the local mean curvature, δ is the Dirac delta function, ϕ is the level set function - which will be further discussed in a subsequent section- and $\hat{\boldsymbol{n}}$ is the unit normal vector outward the droplet surface.

2.2 Nondimensionalization

In order to non-dimensionalize the governing equations, we used the following caracteristics scales: H for length, U for velocity, H/U for time and ρU^2 for pressure. These scales leads to the following nondimensional parameters

$$\tilde{\boldsymbol{u}} = \frac{\boldsymbol{u}}{U}, \;\; \tilde{t} = \frac{Ut}{H}, \;\; \tilde{p} = \frac{p}{\rho U^2}, \;\; \tilde{\nabla} = H\nabla, \;\; \tilde{\kappa} = H\kappa, \;\; \tilde{\delta} = H, \delta \;\; \lambda = \frac{\mu_2}{\mu_1}.$$

Consequently, the Eq. (1) and Eq. (2) in terms of dimensionless group are given by

$$\tilde{\nabla} \cdot \tilde{\boldsymbol{u}} = 0 \tag{4}$$

and

$$\frac{\partial \tilde{\boldsymbol{u}}}{\partial \tilde{t}} + \tilde{\boldsymbol{u}} \cdot \tilde{\nabla} \tilde{\boldsymbol{u}} = -\tilde{\nabla} \tilde{p} + \frac{\lambda}{Re} \tilde{\nabla}^2 \tilde{\boldsymbol{u}} - \frac{1}{Re\, Ca} \kappa \delta(\phi) |\nabla \phi| \hat{\boldsymbol{n}}, \tag{5}$$

where $Re = \frac{\rho_1 U H}{\mu_1}$, $Ca = \frac{\mu_1 U}{\sigma}$ is the Capillary Number and λ is the ratio of viscosity. The Reynolds Number estabilish the ratio between the inertial and viscous effects, and the Capillary Number relates the viscous and the interfacial effects.

3. METHODOLOGY

3.1 Projection Method

We used the Projection Method by Chorin (1968) to split the *Navier-Stokes* equations into two summed up with a Crank-Nicolson scheme proposed by Brown *et al.* (2001) to evolve the solution in time as follow:

$$\frac{\boldsymbol{u}^* - \boldsymbol{u^n}}{\Delta t} = -[\boldsymbol{u} \cdot \nabla \boldsymbol{u}]^{n+\frac{1}{2}} + \frac{\lambda}{2Re} \nabla^2 [\boldsymbol{u}^* + \boldsymbol{u}^n] - \frac{1}{Re\, Ca} [\kappa \delta(\phi) |\nabla \phi| \hat{\boldsymbol{n}}]^{n+\frac{1}{2}} \tag{6}$$

and

$$\frac{\boldsymbol{u}^{n+1} - \boldsymbol{u}^*}{\Delta t} = -\nabla \chi^{n+1}. \tag{7}$$

In Eqs. (6) and (7), $\boldsymbol{u}^*$ is the tentative velocity field and $\boldsymbol{\chi}$ is a virtual(auxiliary) pressure field. The terms valuated at $n + \frac{1}{2}$ are calculated with Adams-Bashforth extrapolation:

$$\boldsymbol{f}^{n+\frac{1}{2}} = \frac{3}{2} \boldsymbol{f}^n - \frac{1}{2} \boldsymbol{f}^{n-1}. \tag{8}$$

By taking the divergence of Eq. (7) and applying the free-divergence condition to the velocity field we obtain a Poisson equation for the virtual (auxiliary) pressure field given by

$$\nabla^2 \chi^{n+1} = \frac{\nabla \cdot \boldsymbol{u}^*}{\Delta t}. \tag{9}$$

3.2 Local Level Set Method

To capture the interface between the fluids, we used a Local Level Set method proposed by Peng *et al.* (1999), which considers evolving a signed distance function ϕ close to the droplet interface. By construction, the points along the droplet interface is set to $\phi = 0$ while outside the droplet is defined with positive values and negative values inside of it. The Local version of the method creates a tube with width γ, such that we can define a *cut-off* function to evolve ϕ inside of it. Therefore,

$$c(\phi) = \begin{cases} 1, & \text{if} \quad |\phi| \leq \beta \\ (|\phi| - \gamma)^2(2|\phi| + \gamma - 3\beta)/(\gamma - \beta)^3, & \text{if} \quad \beta < |\phi| \leq \gamma \\ 0, & \text{if} \quad |\phi| > \gamma, \end{cases} \tag{10}$$

where β defines a inner region inside the tube to provide a smooth transition.

The motion of the interface can be captured by the conservative evolution equation in time given by

$$\frac{\partial \phi}{\partial t} + c(\phi)\boldsymbol{u} \cdot \nabla \phi = 0. \tag{11}$$

Note that Eq. (11) represents the advection of the level set function limited to the region of interest performed by $c(\phi)$ function.

We can also note that the unit normal vector outward the interface can be expressed in terms of the level set function such as

$$\hat{\boldsymbol{n}} = \frac{\nabla \phi}{|\nabla \phi|} \tag{12}$$

and the local mean curvature is given by

$$\kappa = \nabla \cdot \hat{\boldsymbol{n}}. \tag{13}$$

In order to avoid numerical instabilities due to the pressure discontinuity through the interface, we performed a smooth transition of the quantities by considering a finity interface thickness ϵ. To compute that, we defined the Dirac delta function as the derivative of a smoothed Heaviside function as follows:

$$\delta(\phi) = \frac{dH(\phi)}{d\phi} = \begin{cases} 0, & \text{if} \quad \phi < -\epsilon \\ \dfrac{1}{2\epsilon}\left[1 + \cos\dfrac{\pi\phi}{\epsilon}\right], & \text{if} \quad -\epsilon \leq \phi \leq \epsilon \\ 0, & \text{if} \quad \phi > \epsilon, \end{cases} \tag{14}$$

which also provides a smoothed Dirac delta function. The interface thickness was previously set to $\epsilon = 1.5\Delta x$, where Δx is the size of the grid cell.

3.3 Level Set Reinicialization

As Eq. (11) is being advanced in time, the zero contour at the interface is conserved, but the level set function doesn't remain as a signed distance function (Peng *et al.*, 1999). Hence, the level set function must be reinicialized in each time step to keep it as a signed distance function of the points close to the droplet interface. Therefore, the reinicialization of ϕ is performed by solving

$$\frac{\partial \phi}{\partial \tau} + S(\phi)(|\nabla \phi| - 1) = 0, \tag{15}$$

where $S(\phi)$ is a signal function and τ is an artificial time. Equation (15) should be evolved over the artificial time domain until reaching a steady state in order to obtain a new signed distance function for ϕ. Although this technique maintains the level set as a distance function, it can also affect the position of the interface due to numerical errors. So we have to limit the number of reinicializations per time step. In this work, we reinicialized the level set function 3 times per time step.

4. RESULTS AND DISCUSSION

We split the study into two parts: Analyzing the monophasic and biphasic flow in the main channel and analyzing the breakup phenomenon at the T-junction.

4.1 Monophasic flow

First of all, we compared the numerical solution with no drop with the Hagen-Poiseuille flow along two parallel stationary plates, which is described by the parabolic velocity profile

$$\frac{u(y)}{U} = \frac{3}{2}\left[1 - 4\left(\frac{y}{H}\right)^2\right]. \tag{16}$$

Note that Eq. (16) is valid for hydrodynamically fully developed region, after the entrance length region. The maximum velocity is reached at the center of the channel and its value is 1.5, considering the dimensionless velocity $\frac{u(y)}{U}$.

To validate it, we considered a symmetric T-junction with same width H for both the main and the secondary channels. The mass flow that comes from the main channel is divided into two equal channel. This condition guarantees that the velocity profile in the secondaries channel are a half compared to the main channel, so the maximum velocity at the center of these outlet channels reaches 0.75. Table 1 shows the convergence for the maximum velocity in the main channel u_{in} and for the secondary channel u_{out} as the meshgrid was been refined.

Table 1: Convergence of the dimensionless maximum velocity.

Mesh grid	u_{in}	u_{out}	u_{in}/u_{out}
100×100	1,47188	0,730888	2,0138
200×200	1,48691	0,713070	2,0852
300×300	1,48973	0,724473	2,0562
400×400	1,49147	0,745717	2,0000
500×500	1,49173	0,745673	2,0005
600×600	1,49188	0,735967	2,0271

In the Fig. 2, it is displayed isocontour levels for the pressure field perpendicular to the flow direction, which represents the fully developed region where $p = p(x)$.

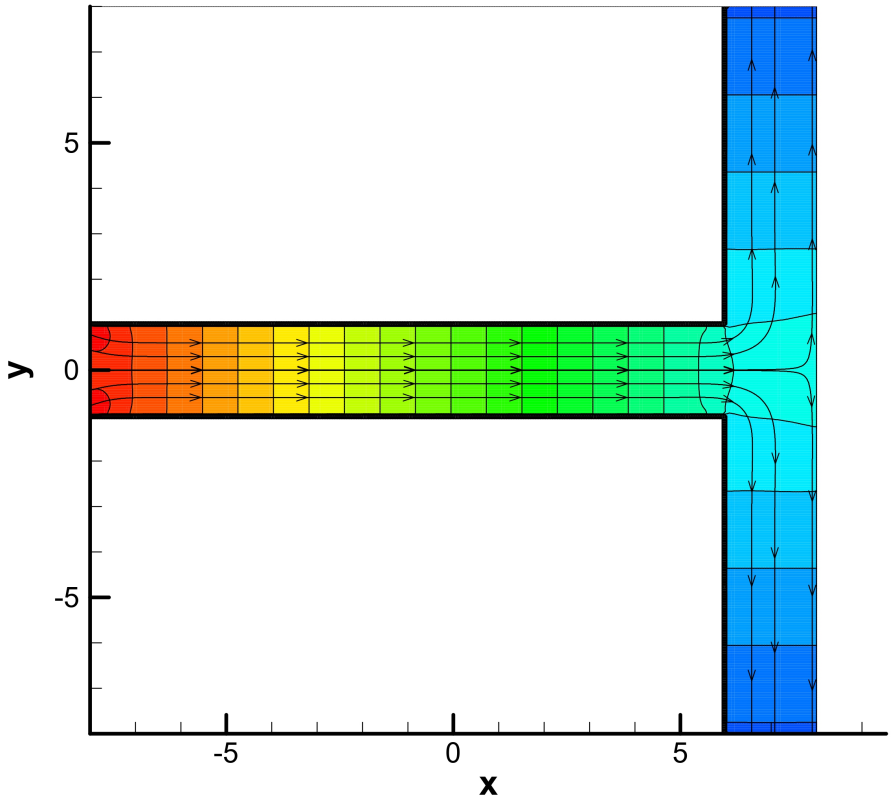

Figure 2: Monophasic flow simulation for $Re = 0.1$ and $L_x = L_y = 16$. The colormap represents the pressure field, where red (higher pressure) and blue (lower pressure).

4.2 Biphasic flow

4.2.1 Effect of confinament

A single circular droplet was placed at the center of the main channel in order to study the effect of the confinament in the droplet shape. For this purpose, we considered 0.075, 0.15 and 0.3 for the aspect ratio a/H, where a is the droplet's radius and H the channel width. To investigate the effect of the Capillary number, we considered values of 0.375, 1.2, 1.5 and 15.02 for it while the Reynolds number was set to 0.5 for all simulations. As shown in Fig. 3, for an aspect ratio of 0.3, which represents a highly confined droplet, the droplet exhibited significant deviation from its initial circular shape at a capillary number of 1.5. However, at a capillary number of 0.375, the deviation was much lesser. This suggests that when interfacial forces are dominant, the effect of confinement has a small impact on the deformation of the droplet. For both cases, the ratio of viscosity was 0.01, which implies that the droplet's fluid has a much lower resistance to flow compared to the surrounding continuous phase. As a result, the droplets are expected to flow more easily and deform more readily. We also compared our simulation with the simulation performed by Afkhami *et al.* (2011), who employed a different numerical methodology. Additionally, we compared it with the theoretical solution proposed by Richardson (1973).

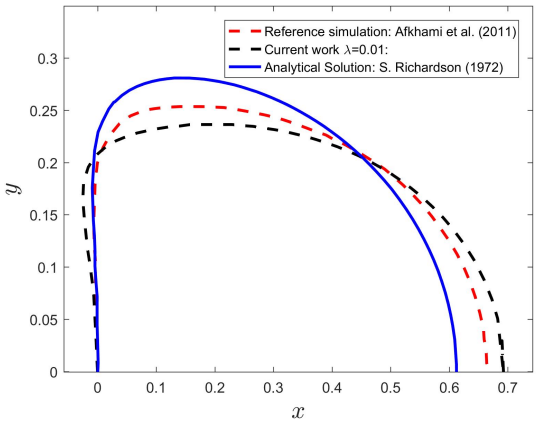

(a) For $Re = 0.5$, $Ca = 1.5$ e $a/H = 0.3$.

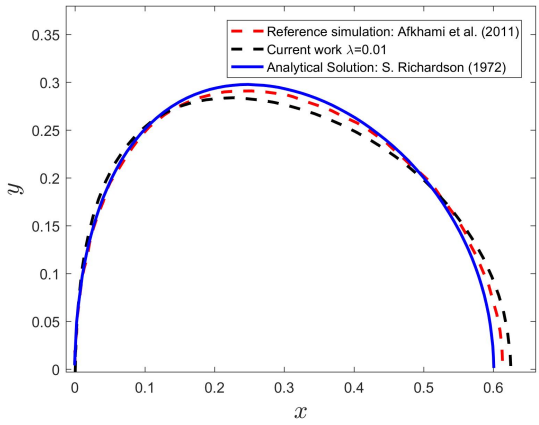

(b) For $Re = 0.5$, $Ca = 0.375$ e $a/H = 0.3$.

Figure 3: Comparison of the droplet contour obtained from the simulation conducted with the results obtained by Afkhami *et al.* (2011) and the theoretical solution developed by Richardson (1973).

In the case of smaller droplets characterized by aspect ratios of 0.15 and 0.075, the simulation demonstrated small deformation at a capillary number of 1.2. For these simulations we employed a unitary ratio of viscosity, which represents that both the inner and the outer fluid offer equal resistance to flow. However, a significant deformation was observed at a capillary number of 15.02. This occurs because surface tension has a lesser impact in restoring the droplet's shape and resisting deformation. Both results showed good agreement with reference solutions, as depicted in Fig. 4.

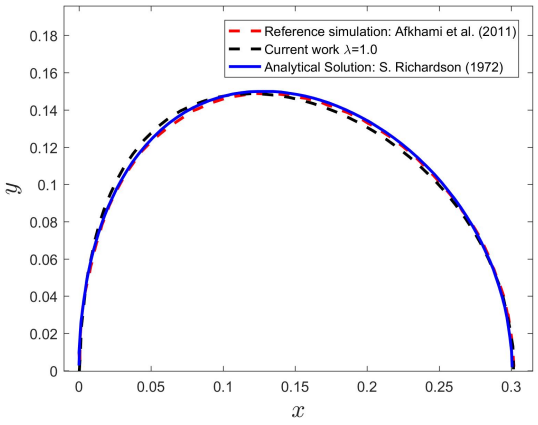

(a) For $Re = 0.5$, $Ca = 1.2$ e $a/H = 0.15$.

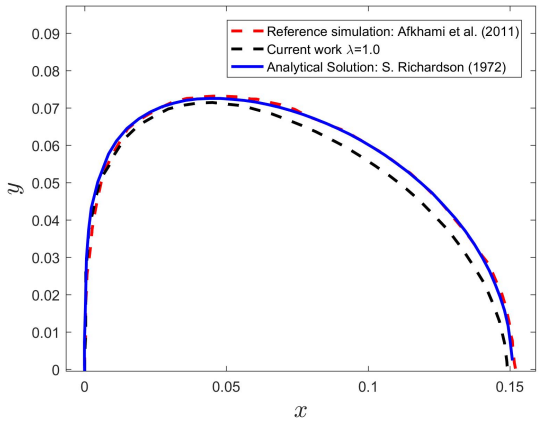

(b) For $Re = 0.5$, $Ca = 15.02$ e $a/H = 0.075$.

Figure 4: Comparison of the droplet contour obtained from the simulation conducted with the results obtained by Afkhami *et al.* (2011) and the theoretical solution developed by Richardson (1973).

4.3 Elongated droplets at the main channel

We also performed simulations for elongated droplets where $2b = H$ and $2a > 2b$, producing elliptical droplets at the center of the main channel. When these elliptical droplets are introduced into the flow, they undergo relaxation and adopt a distinct elongated shape, differing from their initial ellipse. We evaluated the influence of the capillary number in the droplet's velocity as illustrated in Fig. 5. The results indicate that elongated droplets move faster compared to the surrounding fluid. The analytical solution proposed by Hodges *et al.* (2004) is applicable to a 2D droplet undergoing Poiseuille flow in a slit channel, assuming an intermediate viscosity ratio between the fluids.

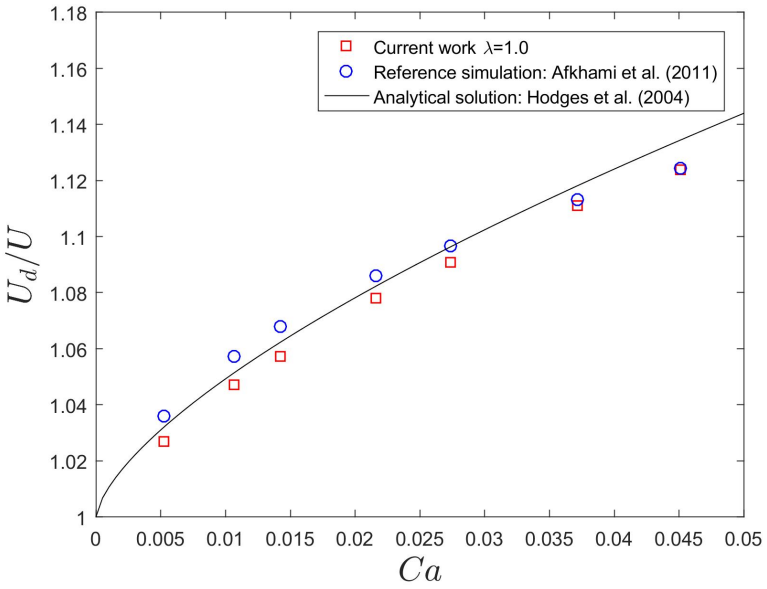

Figure 5: Relation between the droplet's velocity normalized by the mean flow velocity and the capillary number for $\lambda = 1.0$. The solid line represents the solution given by $\dfrac{U_d}{U} \approx 1 + 0.51(3Ca)^{2/3}$.

4.4 Droplet breakup

In the Fig. 6, we present a visual comparative analysis between our simulation and the work of Afkhami *et al.* (2011). To replicate a similar scenario, we adjusted the parameter $2a$ to match the initial droplet length ℓ_0 defined by Afkhami et al. However, in Fig. 6d, we see that the maximum extension of the drop reached in our simulation is less compared to the reference. In fact, the relation $2a = \ell_0$ doesn't match, since $2a$ is the length of an elipse and ℓ_0 is the initial length of the droplet after a relaxation time.

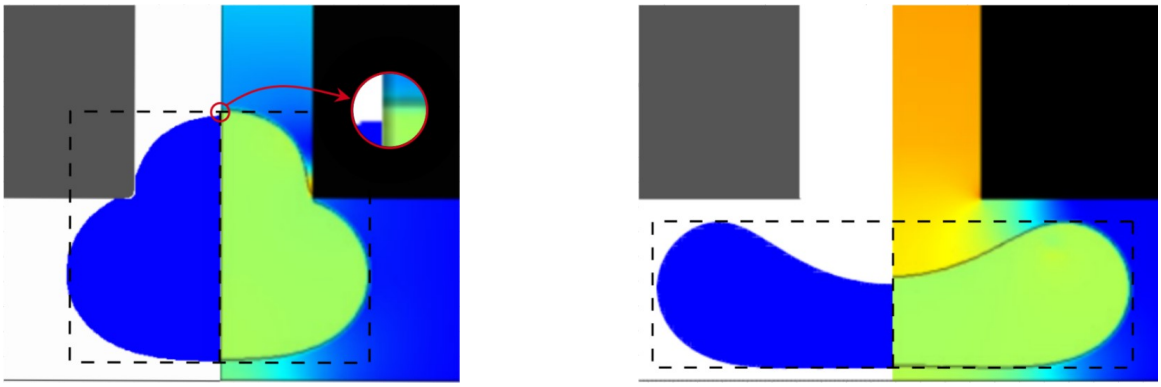

(a) (b)

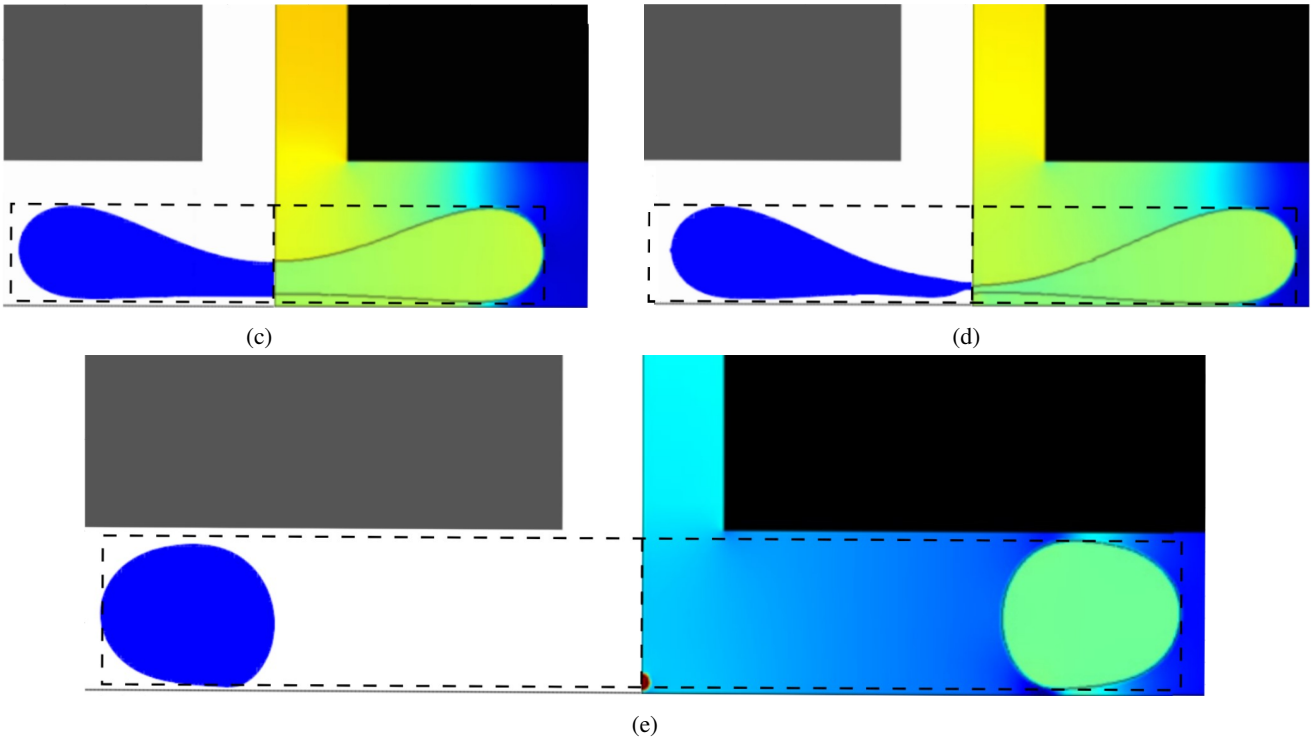

Figure 6: Comparison between the simulation conducted in this study (left half) and the simulation performed by Afkhami *et al.* (2011) (right half) for $Re = 0.5$, $Ca = 0.05$, $\ell_0/H = 2.0$ and $\gamma = 0.1$.

In order to resolve this inconsistency, we run some simulations for a range of $2a$ to obtain a more apropriated parameter to represent the initial droplet's length of Afkhami et al. The relation is given by

$$\frac{\ell}{H} \approx 2.06 \left(\frac{2a}{H}\right) + 0.28, \tag{17}$$

where ℓ is the maximum extension of the droplet just before the breakup. It is depicted in Fig. 7 a correction in the maximum extension of the droplet for $2a/H \approx 2.05$, provided by Eq. 17, resulting in a highly agreement with Afkhami's.

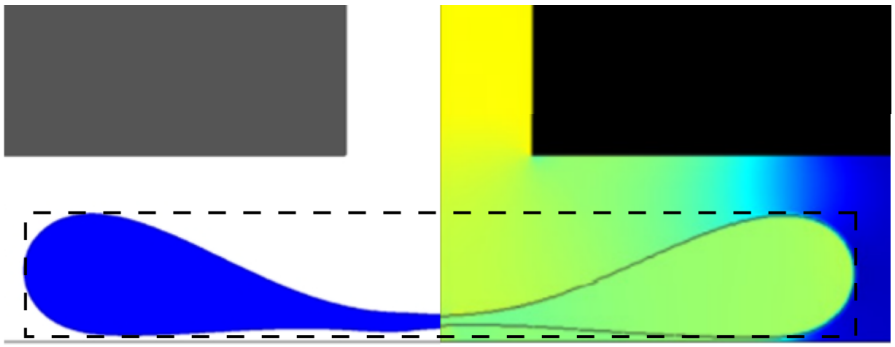

Figure 7: Correction (left half) by using the relationship between ℓ and $2a$ to obtain the maximum droplet extension before rupture. The green half-droplet (right half) corresponds to the simulation by Afkhami *et al.* (2011).

We also measured the film thickness δ when the droplet undergoes breakup in regime with tunnel and it reaches its maximum extension in the T-junction. Figure 8 presents the correlation between the film thickness and the capillary number under a unitary viscosity ratio. It is observed that, for larger capillary numbers, the film thickness obtained in our simulations does not agree well with the results obtained by Afkhami *et al.* (2011), likely due to the additional influence of the Reynolds number that they can be used but it is not avaiable in their work for a more accurate comparison. However, at lower capillary numbers, our results are consistent with the theoretical model proposed by Leshansky and Pismen (2009), which was demonstrated that the film thickness scales with $Ca^{2/5}$ and is given by

$$\delta/H \approx 1.08 Ca^{2/5}. \tag{18}$$

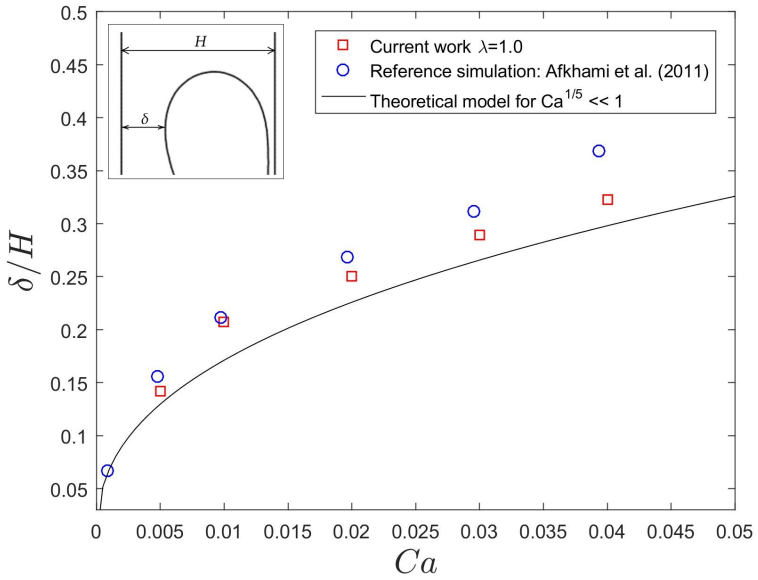

Figure 8: The relationship between the film thickness δ and the capillary number for the simulations conducted in this study and those performed by Afkhami *et al.* (2011) for $\lambda = 1.0$ is shown. The solid curve corresponds to the theoretical equation given by Eq. 18.

For the purpose of comparing with the real physics, we compared our results with experimental data. One of the experiments performed by Jullien *et al.* (2009) used fluorinated oil droplets in de-ionized water with 1% w/w sodium dodecyl sulfate with $\lambda = 1.67$ to provide the relation between the film thickness and the capillary number. We show in Fig. 9 the comparison of our work with Jullien's. It is noticeable that there is a relatively large standard deviation, although the majority of the simulations conducted agree with the experimental results within the uncertainty range.

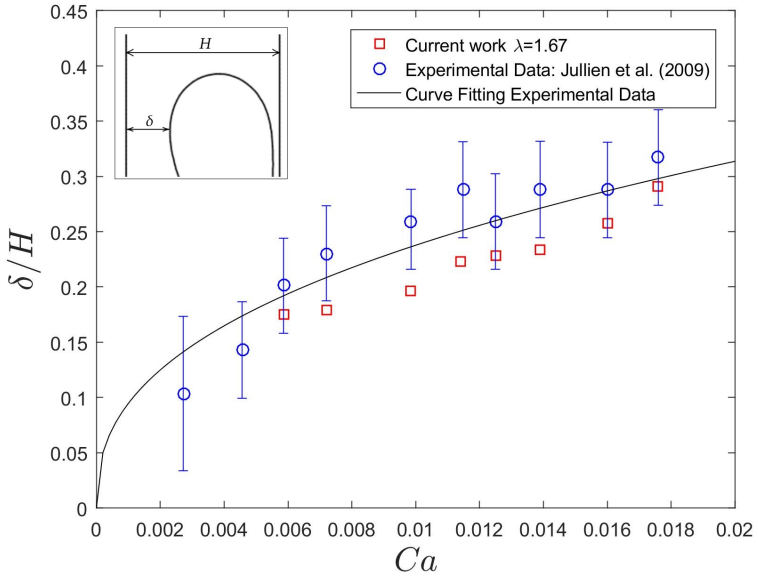

Figure 9: Relationship between the film thickness δ and the capillary number for the simulations conducted in this work and the experiments by Jullien *et al.* (2009). The solid curve represents a fit to the experimental data.

5. Conclusion

In this work we presented a numerical model considering the Navier-Stokes equation for incompressible transient flow and the level set method to capture the interface of a droplet along a T-Junction. We presented a variety of comparisons in order to validate our approach with reference from the literature. Our results presented very good agreement with numerical references and theoretical model for the droplet shape in the main channel before the T-junction. We also

discussed the influence of the confinament combined with the capillary number on the shape of the droplet. Additionally, we showed that elongated droplets move faster than the surrounding fluid in the main channel, demonstrating excelent agreement with the theory. For breakup analysis, our results fit with the reference for the droplet shape and deformation. Moreover, we discussed the effect of the capillary number in the maximum gap between the interface and the channel wall before the rupture showing good agreement with the references and the theory.

Furthermore, our proposed methodology demonstrates its efficacy in studying droplet deformation and breakup in T-junctions, opening possibilities for future research in this field. This work could be extended to three-dimensional configuration in order to investigate the impact of additional factors such as the Rayleigh-Plateau instability. Additionally, an exciting prospect for future studies involves the implementation of a magnetic setup to analyze the behavior of ferrofluid droplets under the influence of an external magnetic field. These potential research directions hold promise for advancing our understanding of droplet dynamics and enhancing the applicability of our findings in various fields.

6. REFERENCES

Afkhami, S., Leshansky, A. and Renardy, Y., 2011. "Numerical investigation of elongated drops in a microfluidic t-junction". *Physics of Fluids - PHYS FLUIDS*, Vol. 23. doi:10.1063/1.3549266.

Brown, D.L., Cortez, R. and Minion, M.L., 2001. "Accurate projection methods for the incompressible navier–stokes equations". *Journal of Computational Physics*, Vol. 168, No. 2, pp. 464–499. ISSN 0021-9991. doi:https://doi.org/10.1006/jcph.2001.6715. URL `https://www.sciencedirect.com/science/article/pii/S0021999101967154`.

Chorin, A.J., 1968. "Numerical solution of the navier-stokes equations". *Mathematics of Computation*, Vol. 22, No. 104, pp. 745–762. ISSN 00255718, 10886842. URL `http://www.jstor.org/stable/2004575`.

Hodges, S.R., Jensen, O.E. and Rallison, J.M., 2004. "The motion of a viscous drop through a cylindrical tube". *Journal of Fluid Mechanics*, Vol. 501, p. 279–301. doi:10.1017/S0022112003007213.

Jullien, M.C., Ching, M.J.T.M., Cohen, C., Ménétrier, L. and Tabeling, P., 2009. "Droplet breakup in microfluidic t-junctions at small capillary numbers". *Physics of Fluids*, Vol. 21, p. 072001.

Leshansky, A. and Pismen, L., 2009. "Breakup of drops in a microfluidic t junction". *Physics of Fluids - PHYS FLUIDS*, Vol. 21. doi:10.1063/1.3078515.

Link, D.R., Anna, S.L., Weitz, D.A. and Stone, H.A., 2004. "Geometrically mediated breakup of drops in microfluidic devices". *Phys. Rev. Lett.*, Vol. 92, p. 054503. doi:10.1103/PhysRevLett.92.054503. URL `https://link.aps.org/doi/10.1103/PhysRevLett.92.054503`.

Peng, D., Merriman, B., Osher, S., Zhao, H. and Kang, M., 1999. "A pde-based fast local level set method". *Journal of Computational Physics*, Vol. 155, No. 2, pp. 410–438. ISSN 0021-9991. doi:https://doi.org/10.1006/jcph.1999.6345. URL `https://www.sciencedirect.com/science/article/pii/S0021999199963453`.

Richardson, S., 1968. "Two-dimensional bubbles in slow viscous flows". *Journal of Fluid Mechanics*, Vol. 33, No. 3, p. 475–493. doi:10.1017/S0022112068001461.

Richardson, S., 1973. "Two-dimensional bubbles in slow viscous flows. part 2". *Journal of Fluid Mechanics*, Vol. 58, No. 1, p. 115–127. doi:10.1017/S0022112073002168.

Taylor, G.I., 1932. "The viscosity of a fluid containing small drops of another fluid". *Proceedings of the Royal Society of London. Series A, Containing Papers of a Mathematical and Physical Character*, Vol. 138, No. 834, pp. 41–48. ISSN 09501207. URL `http://www.jstor.org/stable/96007`.

Taylor, G.I.S., 1934. "The formation of emulsions in definable fields of flow". *Proceedings of The Royal Society A: Mathematical, Physical and Engineering Sciences*, Vol. 146, pp. 501–523.

7. RESPONSABILITY NOTICE

The authors are the only responsible for the printed material included in this paper.